Supporting Information

Twin-Axial Pseudorotaxane for Phosphorescence Cell Imaging

Experimental

General: All reagents and solvents were commercially available and used without further purification, unless otherwise noted. NMR spectra were recorded on an Ascend 400 MHz instrument. High-resolution mass (HR-MS) spectra were performed on a Q-TOF LC-MS with an ESI mode. Absorption spectra were record on a Thermo Fisher Scientific EVO300 PC spectrophotometer in a conventional rectangular quartz cell (10 × 10 × 45 mm) at 25 °C. The photoluminescence spectra and fluorescence/phosphorescence lifetimes were measured by time-correlated single photon counting on a FLS980 instrument (Edinburg Instruments Ltd., Livingstone, UK). Phosphorescence quantum efficiency were measured on F980. Trans-mission electron microscopy (TEM) experiments were accomplished on FEI Tecnai G2 F20 under 200KV. Laser scanning confocal microscope (LSCM) images were obtained on Leica TCS SP8.

ITC Measurements. ITC measurements were performed with an isothermal titration microcalorimeter (VP–ITC, Microcal Inc.) at atmospheric pressure and 25.00 °C in aqueous solution to obtain stability constants (K_S) and thermodynamic parameters. A solution of BrBP–NH_2 in a 0.250 mL syringe was sequentially injected into a stirring (300 rpm) solution of CB[7, 8] in the sample cell (1.4227 mL volume). The concentrations of CB[7] and BrBP–NH_2 were used as 0.048 and 1.25 mM, respectively. The thermodynamic parameters were obtained by using a model with one set of binding sites. The concentrations of CB[8] and BrBP–NH_2 were used as 0.040 and 1.28 mM, respectively. The thermodynamic parameters reported in this work were obtained by using a sequential binding sites model with 1:2 stoichiometry.

Theoretical calculation: To further understand unique phosphorescence, density functional theory (DFT) and time-dependent density functional theory (TD-DFT) calculations were carried out. All the molecules in ground states (S_0) were optimized by using the M06-2X-GD3[1,2] functional along with the 6-31G(d,p)[3] basis set. Based on the S_0 geometries, the single point energies and frontier molecular orbital (FMO) were calculated using the M06-2X-GD3 and 6-311G(d,p)[3] basis set in water solvent with the SMD solvation model[4], while the excitation energies were calculated by using TD-DFT for excited singlet and triplet states. The above calculations were performed by using the Gaussian 16 Software[5]. At the same level as the excitation energies calculation, the spin–orbit coupling (SOC) between singlet and triplet states were given by ORCA 4.1.2[6]. The optimized structures were rendered using CYLView software.

Synthesis

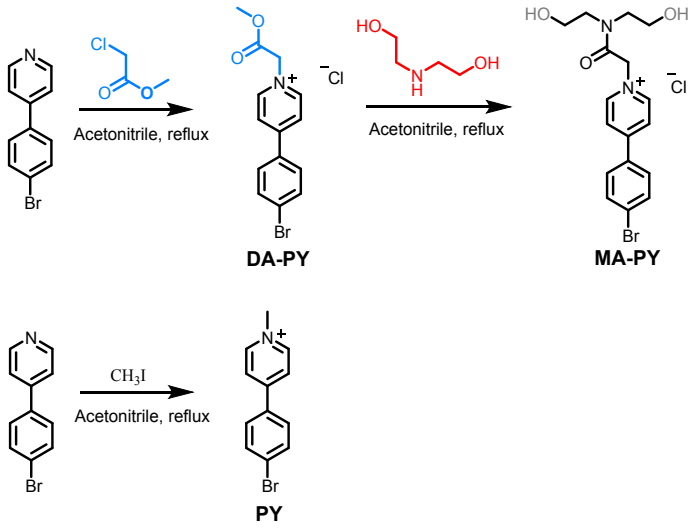

Scheme S1. Synthetic route of the compounds.

Syntheses of MA-PY and DA-PY: 4-(4-bromophenyl) Pyridine (1.00 g, 4.27 mmol) and methyl chloroacetate (0.51 mg, 4.70 mmol) were added to acetonitrile (25 mL) and refluxed for 12h. Then the mixture was filtered and washed with acetonitrile (2 × 10 mL) to afford pure product as white solid (1.20 g, 82%). ^{1}H NMR (400 MHz, D_2O): 8.78(d, J=7.08,2H), 8.34(d, J=7.08,2H), 7.82(q, J=9,4H), 5.55(s,2H),3.86(s,3H) ppm; ^{13}C NMR (101 MHz, D_2O) δ 167.83, 156.21, 145.55, 132.74, 132.12, 129.54, 126.99,124.44; HRMS (*m/z*): $[M\text{-}Cl]^+$ calc. for $C_{14}H_{13}NO_2Br$, 306.0124; found, 306.0127.

MA-PY (1.00 g, 4.27 mmol) and diethanol amine (0.51 mg, 2.0 mmol) were added to acetonitrile (10 mL) and refluxed for 12h. The mixture was precipitated in acetonitrile (50 mL) and filter, then repeated several times until residue is no longer oily, the pure product is yellow solid (800mg, 66%). ^{1}H NMR (400 MHz, D_2O): 8.68(d, J=6.56,2H),8.28(d, J=6.52,2H), 7.78(q, J=8.68,4H), 3.85(t, J=5.08,2H), 3.75(t, J=5.56, 2H), 3.66(t, J=5.08,2H), 3.60(t, J=5.56, 2H) ppm; ^{13}C NMR (101 MHz, D_2O) δ 166.61, 155.58, 145.66, 132,67, 129.43, 126.87, 124.01,58.43, 49.75, 48.24; HRMS (*m/z*): $[M\text{-}Cl]^+$ calc. for $C_{17}H_{20}N_2O_3Br$, 379.0652; found, 379.0655.

PY was synthesized according to the literature.

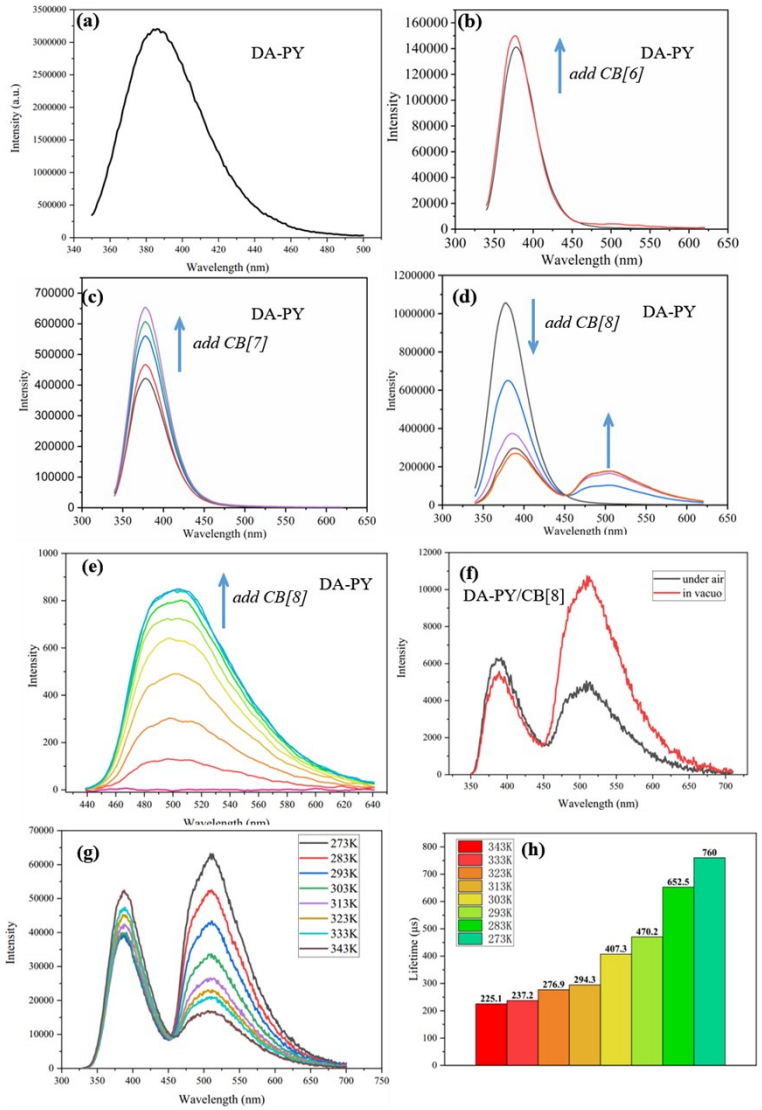

Figure S1. (a) DA-PY (1.00 mM) in aqueous solution at 298K; (b) DA-PY (1.00 mM) upon addition of CB[6] in aqueous solution at 298K; Note that because of poor solubility of CB[6], the clear solution of DA-PY/CB[6] could not be obtained even mixture was heated and ultrasound for days, therefore DA-PY and excess CB[6] (1.2 equiv.) were mixed and dissolved for 24 h then filtered to get a clear solution. (c) DA-PY (1.00 mM) upon addition of CB[7] (0−1.0 mM), in aqueous solution at 298K; (d) DA-PY (1.00 mM) upon addition of CB[8] (0−0.75 mM), in aqueous solution at 298K; (e) alterations of the phosphorescence emission spectra (delayed 0.1 ms) of DA-PY (10 μM) upon addition of CB[8] (0−8 μM), in aqueous solution at 298 K; (f) Fluorescence spectra of DA-PY/CB[8] solution ([CB[8]] = 0.3 mM and [DA-PY] = 0.6 mM) at room temperature under air (black) and after vacuum deoxy (red); (g) Fluorescence emission spectra at different temperature (from 279 to 343 K of DA-PY/CB[8] solution([CB[8]] = 30 μM and [DA-PY] = 60 μM); (h) Phosphorescence lifetime of DA-PY/CB[8] solution ([CB[8]] = 30 μM and [DA-PY] = 60 μM) at 510 nm at different temperature (from 279 to 343 K). Note: DA-PY upon adding CB[6, 7, 8] spectrums were excited by 325 nm.

Table S1. Photophysical data of DA-PY and DA-PY/CB[n], MA-PY and MA-PY/CB[n].

Compound	E_X (nm)	λ_{Fluo} (nm)	λ_{Phos} (nm)	τ_{Fluo} (μs)	τ_{phos} (μs)	k_{isc} (s^{-1})
DA-PY	310	384	\	8.61	\	\

DA-PY/CB[6]	310	384	\	8.29	\	\
DA-PY/CB[7]	315	389	\	7.56	\	\
DA-PY/CB[8]	314	379	503	13.73	419/1690 (solid state)	1988
MA-PY	310	385	\	9.17	\	\
MA-PY/CB[6]	310	386	\	8.34	\	\
MA-PY/CB[7]	315	386	\	7.98	\	\
MA-PY/CB[8]	315	389	506	10.06	372	1690
PY	315	378	\	\	\	\
PY/CB[8]	307	386	502	12.56	264	908
\:not detected $k_{ISC}= \Phi_{Phos}/\tau_{Fluo}$.						

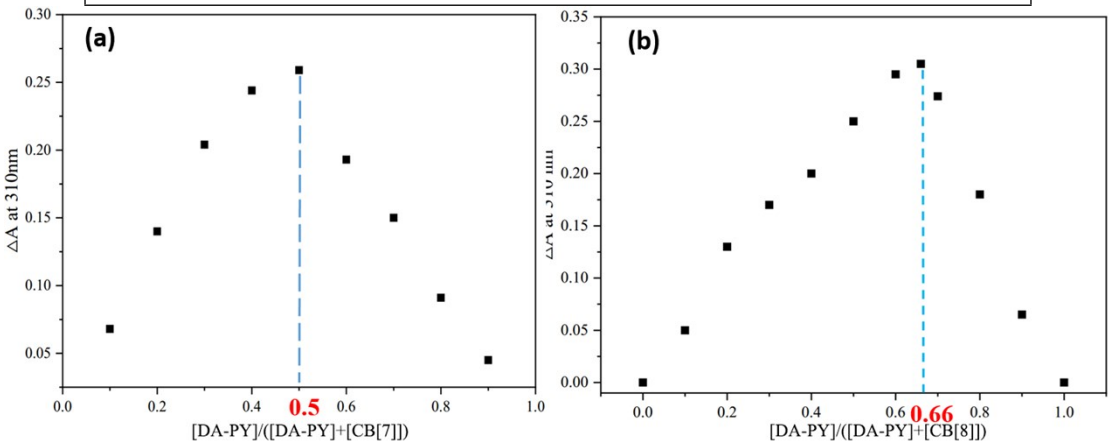

Figure S2. Job's experiment for DA-PY upon complexation with CB[8] and CB[7] in aqueous solution at 298 K. Absorbance intensity changes of DA-PY recorded at 310 nm was used to analyze the binding ratio. (a)the total concentration of host and guest is constant ([DA-PY] + [CB[7]] = 1 mM). (b)the total concentration of host and guest is constant ([DA-PY] + [CB[8]] = 0.1 mM).

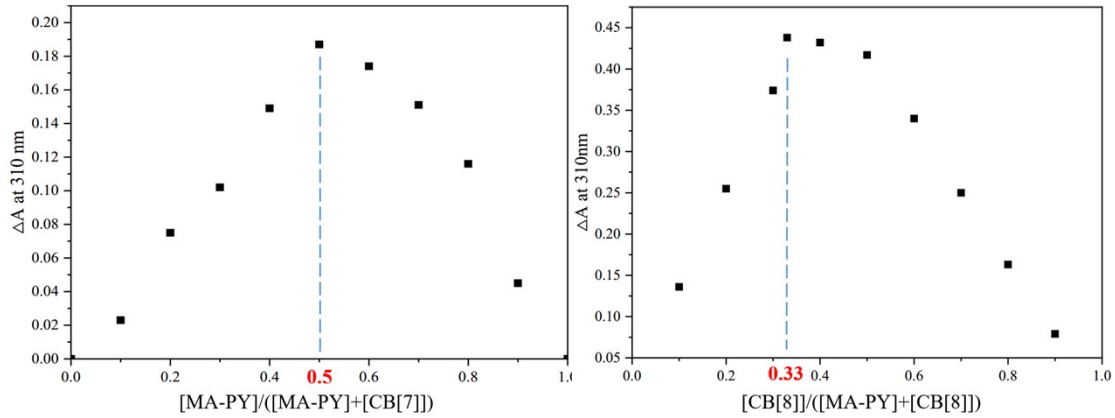

Figure S3. Job's experiment for MA-PY upon complexation with CB[8] and CB[7] in aqueous solution at 298 K. Absorbance intensity changes of DA-PY recorded at 310 nm was used to analyze the binding ratio. (a)the total

concentration of host and guest is constant ([MA-PY] + [CB[7]] = 1 mM). (b)the total concentration of host and guest is constant ([MA-PY] + [CB[8]] = 0.1 mM).

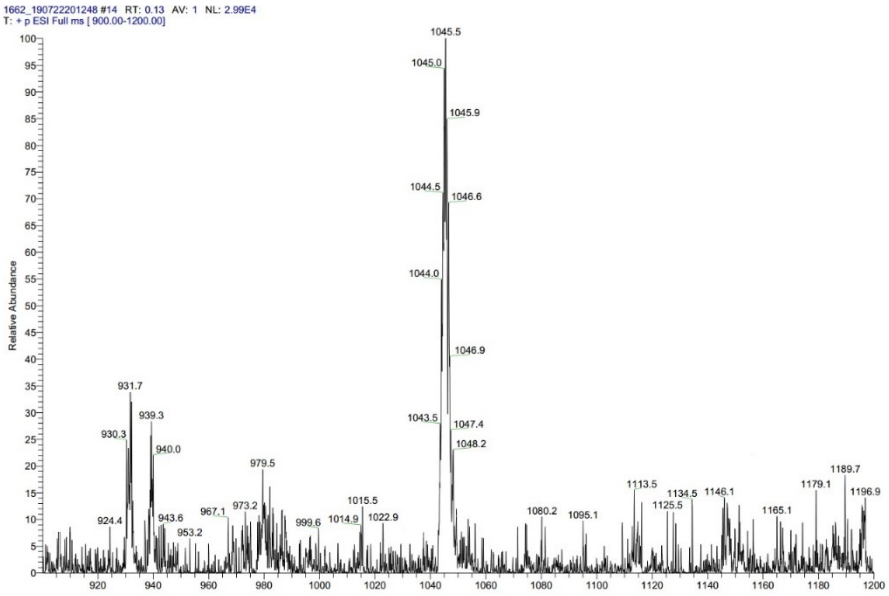

Figure S4. Mass spectrometry of DA-PY/CB[8].

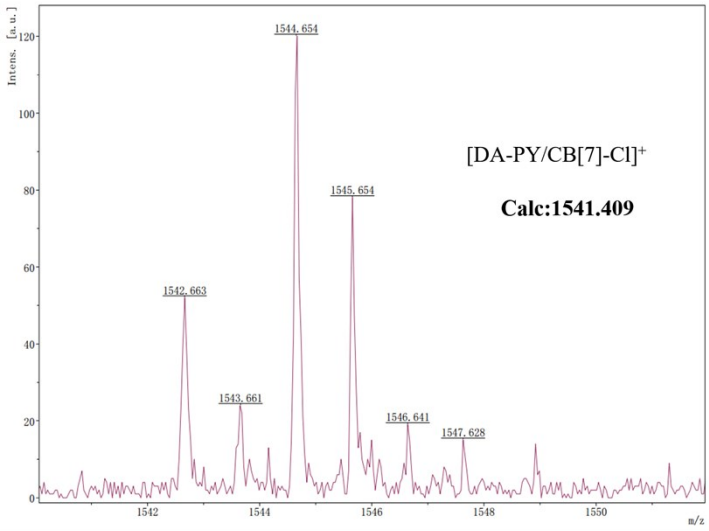

Figure S5. Mass spectrometry of DA-PY/CB[7].

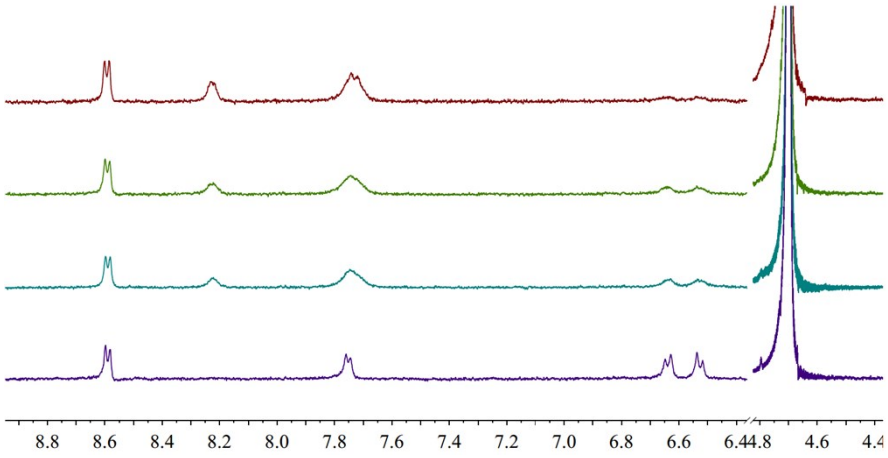

Figure S6. ^{1}H NMR (400 MHz, D_2O, 298 K) spectra in solution of DA-PY (10.0 μM) upon addition of CB[8] (2.00,3.00,4.00,5.00 μM)

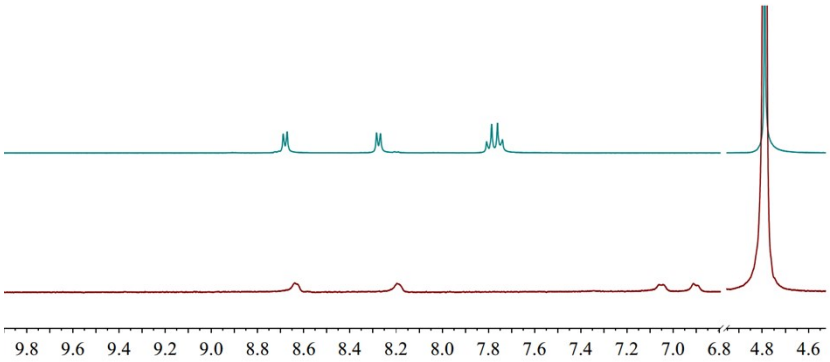

Figure S7. ^{1}H NMR (400 MHz, D_2O, 298 K) spectra in solution of DA-PY/CB[7] (maroon) (10.0 μM/10.0 μM) and DA-PY (green) (10.0 μM).

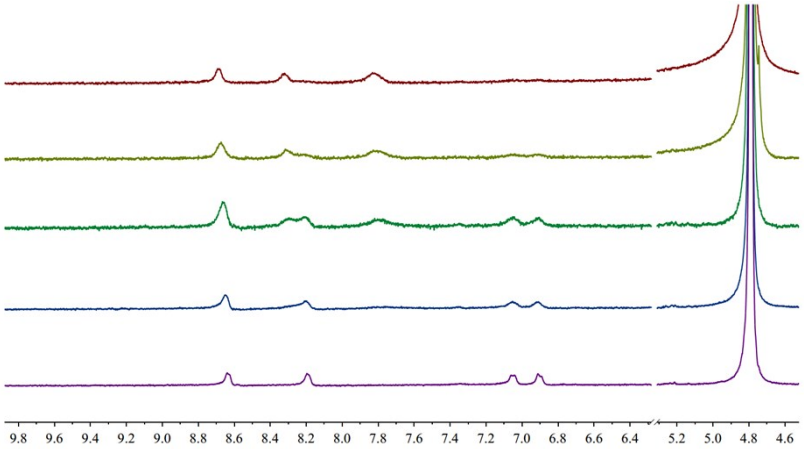

Figure S8. ^{1}H NMR (400 MHz, D_2O, 298 K) spectra in solution of DA-PY (10.0 μM) upon addition of CB[7] (2.00,4.00,6.00,8.00,10.0 μM)

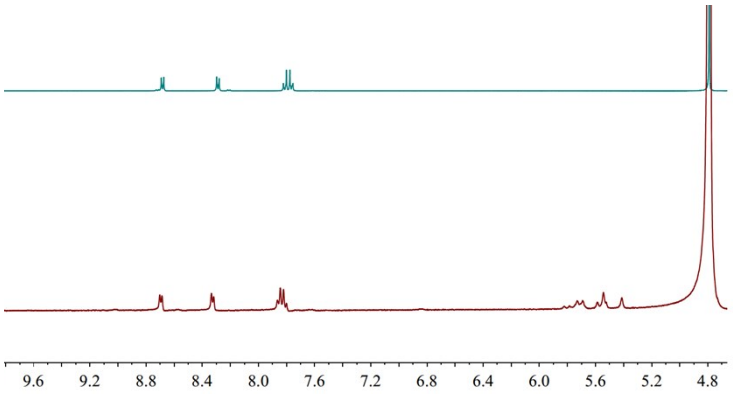

Figure S9. ^{1}H NMR (400 MHz, D_2O, 298 K) spectra in solution of DA-PY (top) and DA-PY/CB[6] (10.0 μM).

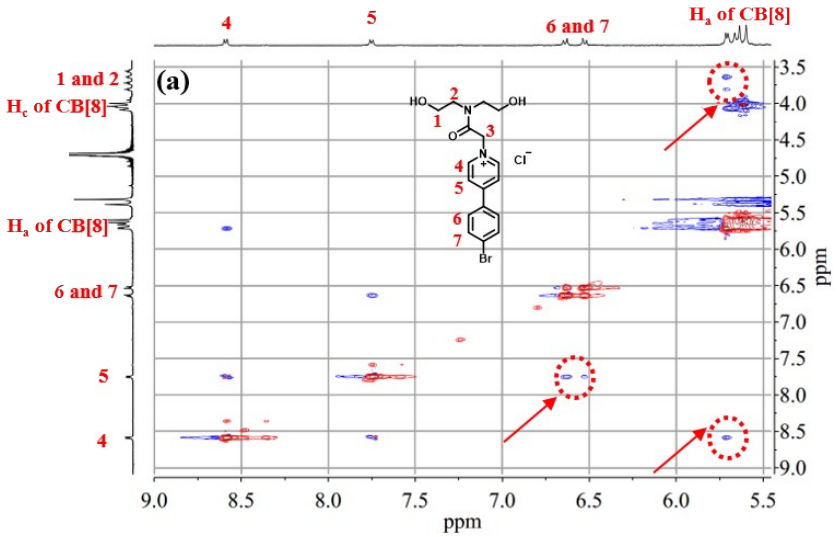

Figure S10. 2D ROESY Spectrum (400 MHz, D_2O, 298 K) of DA-PY/CB[8] ([DA-PY] = 5.0 mM, [CB[8]] = 2.5 mM).

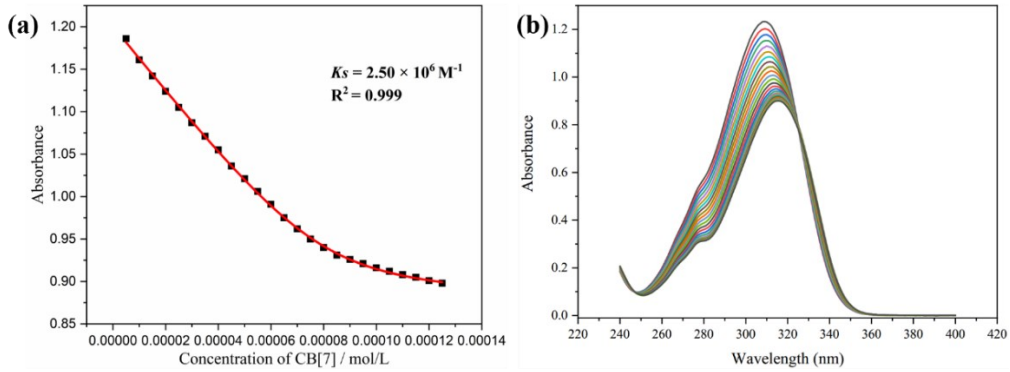

Figure S11. (a) The nonlinear least-squares analysis of the variation of absorbance with the concentration of CB[7] to calculate the binding constant from the corresponding absorbance in Fig. S11b. (b) UV/Vis spectra of DA-PY (0.02 mM) with varying concentrations of CB[8] from 0 to 0.03 mM in aqueous solution at 298 K.

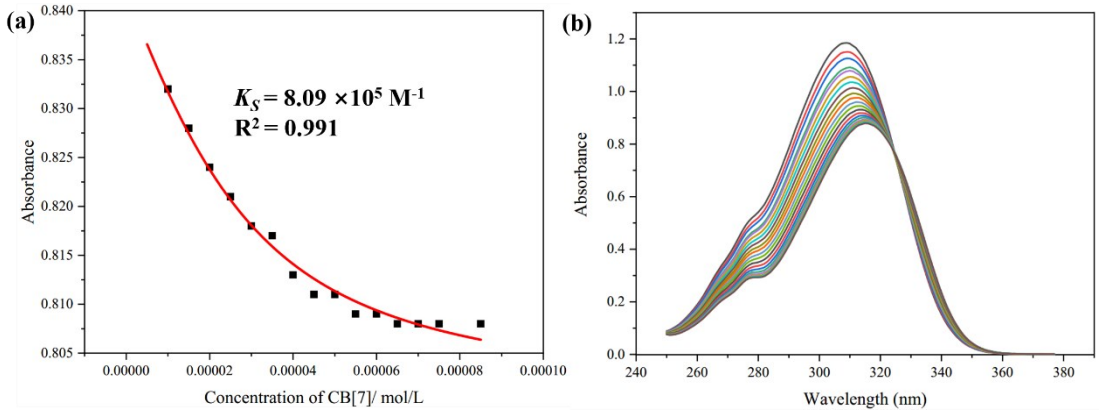

Figure S12. (a) The nonlinear least-squares analysis of the variation of absorbance with the concentration of CB[7] to calculate the binding constant from the corresponding absorbance in Fig. S12b. (b) UV/Vis spectra of MA-PY (0.02 mM) with varying concentrations of CB[8] from 0 to 0.03 mM in aqueous solution at 298 K.

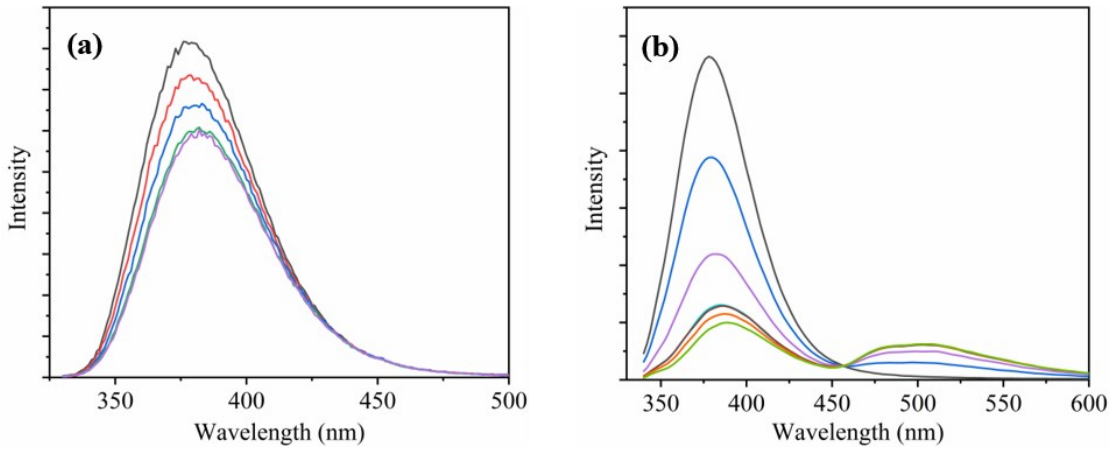

Figure S13. Alterations of the fluorescence emission spectra in aqueous solution at 298K: (a) MA-PY (1.00 mM) upon addition of CB[7] (0−1.0 mM); (b) MA-PY (1.00 mM) upon addition of CB[8] (0−1.0 mM). Note: DA-PY upon adding CB[6, 7, 8] spectrums were excited by 325 nm.

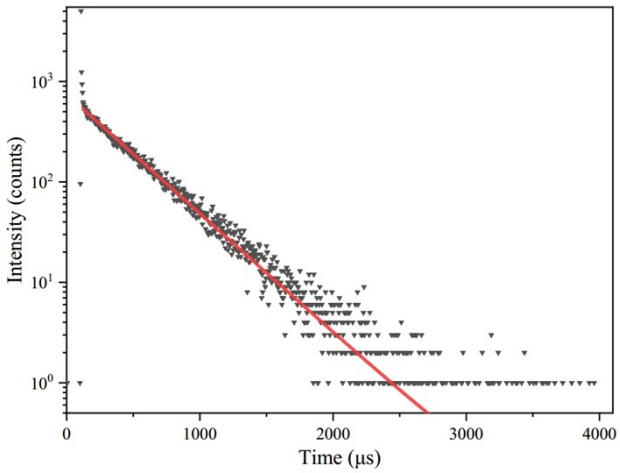

Figure S14. Time-resolved PL decay of MA-PY at room temperature under air ([CB[8]] =30 μM and [MA-PY] = 60 μM)

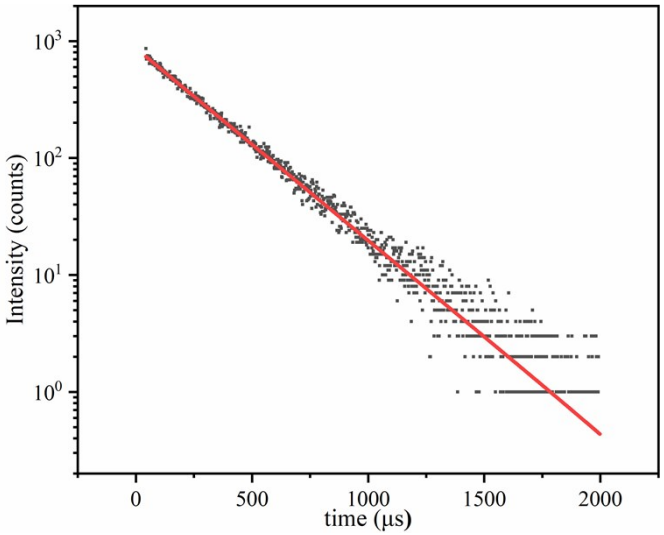

Figure S15. Time-resolved PL decay of PY at room temperature under air([CB[8]] =30 μM and [PY] = 60 μM).

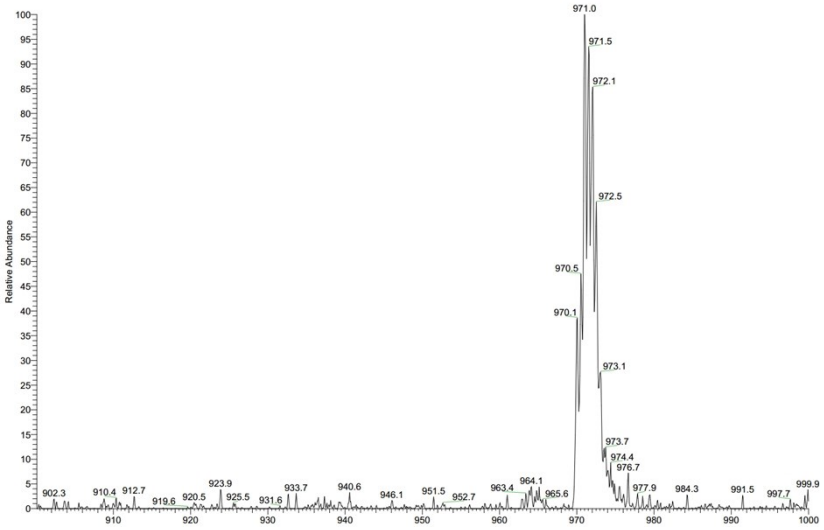

Figure S16. Mass spectrometry of MA-PY/CB[8]

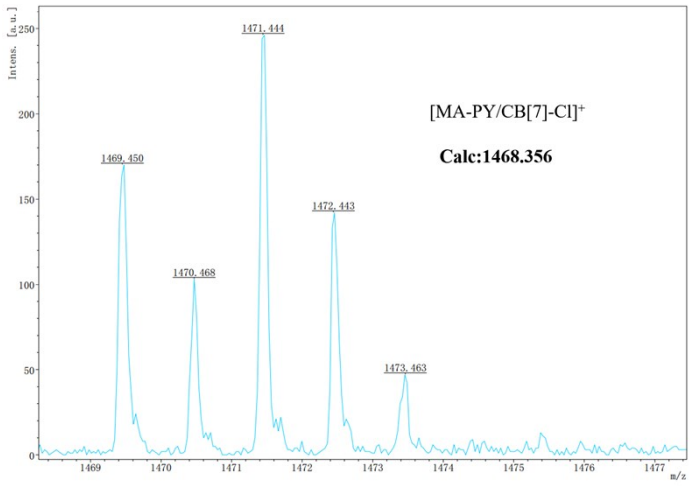

Figure S17. Mass spectrometry of MA-PY/CB[7]

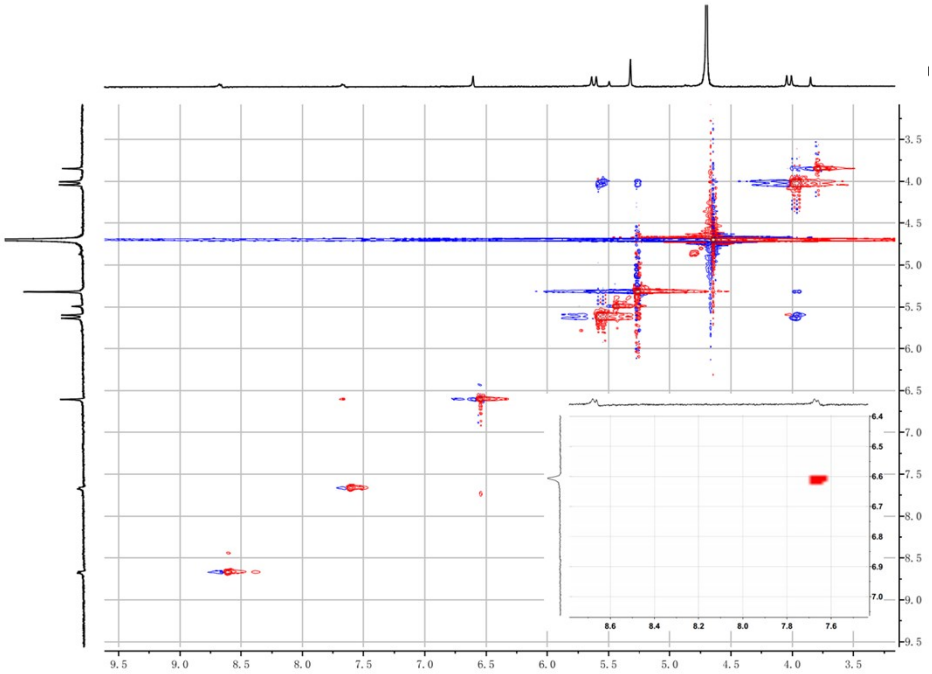

Figure S18. 2D ROESY Spectrum (400 MHz, D_2O, 298 K) of MA-PY/CB[8] ([MA-PY] = 5.0 mM,[CB[8]] = 2.5 mM).

Table S1. Energy level transition data of DA-PY/CB[8]

DA-PY/CB[8]				MA-PY/CB[8]				DA-PY			
Energy level	Energy/eV	Energy level	Energy/eV	Energy level	Energy/eV	Energy level	Energy/eV	Energy level	Energy/eV	Energy level	Energy/eV
S_1	4.0090	T_1	3.1972	S_1	4.2198	T_1	3.3066	S_1	4.4095	T_1	3.3884
S_2	4.3141	T_2	3.2019	S_2	4.4101	T_2	3.3185	S_2	4.9414	T_2	4.1557
S_3	4.5366	T_3	3.9372	S_3	4.7218	T_3	3.9674	S_3	5.1605	T_3	4.4515
S_4	4.6436	T_4	3.9536	S_4	4.7426	T_4	3.9683	S_4	5.2715	T_4	4.5022
S_5	4.7275	T_5	4.2443	S_5	4.7795	T_5	4.2403	S_5	5.7678	T_5	4.7910

Table S2. The single point energy of the optimized structure

	DA-PY/CB[8]	MA-PY/CB[8]	DA-PY
SPE/hartree	-11951.850178	-11454.886039	-3568.923975
LUMO	-0.06243	-0.06531	-0.06306
HOMO	-0.28226	-0.29498	-0.29927
gap/eV	5.98	6.25	6.43

Luminescent property data.

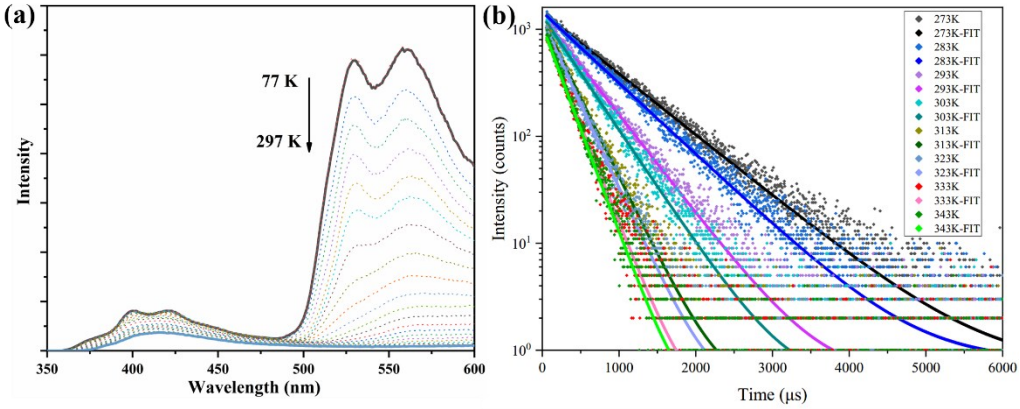

Figure S19. (a) Fluorescence emission spectra of DA-PY in the solid state at different temperature under air. (b) Time-resolved PL decay of DA-PY/CB[8] at different temperature under air.

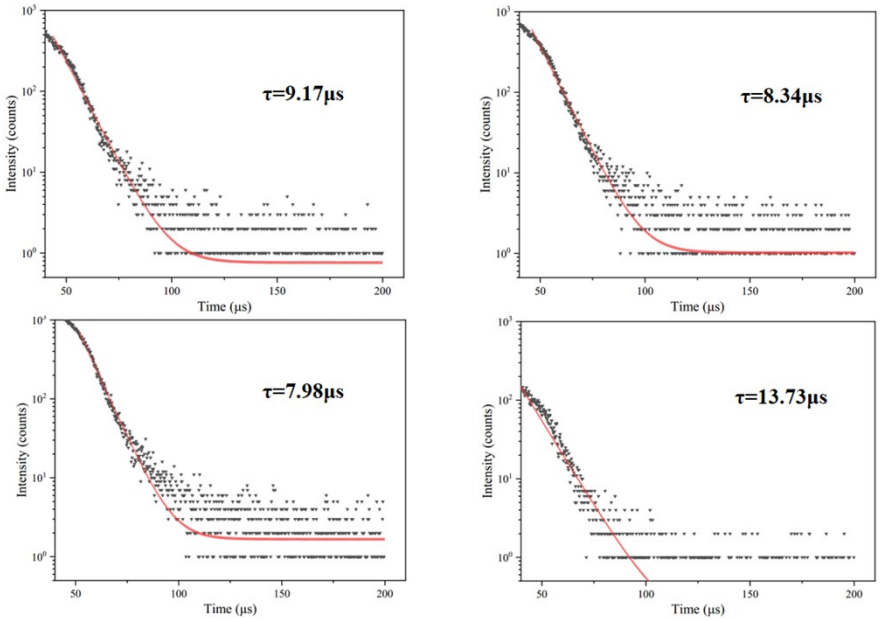

Figure S20. Time-resolved PL decay at room temperature under air: (a)MA-PY; (b) MA-PY/CB[6]; (c) MA-PY/CB[7] ; Time-resolved decay at room temperature under air: (d) DA-PY/CB[8]

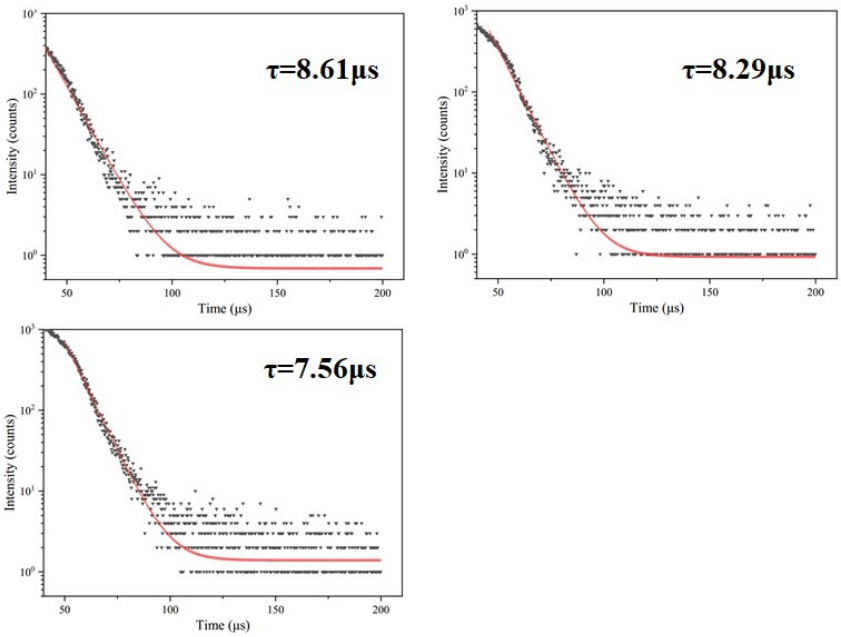

Figure S21. Time-resolved PL decay at room temperature under air: (a)DA-PY; (b) DA-PY/CB[6]; (c) DA-PY/CB[7].

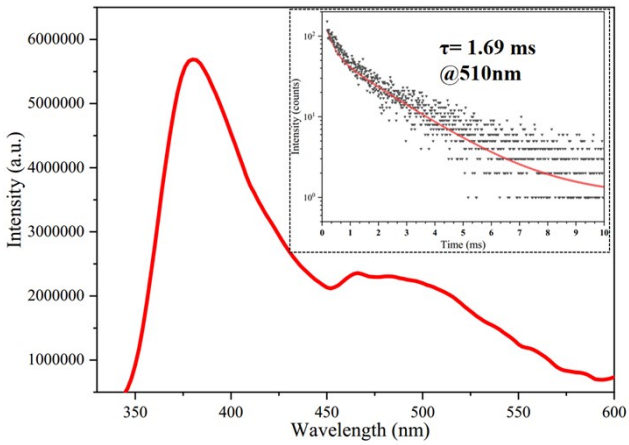

Figure S22. Fluorescence emission spectra of DA-PY/CB[8] in solid state at RT. (dissolve and lyophilize) and time-resolved PL decay of DA-PY/CB[8] in solid state at room temperature under air (insert).

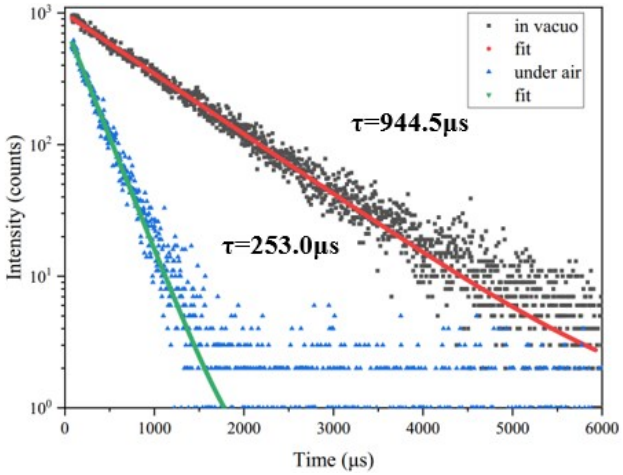

Figure S23. Time-resolved photoluminescence decay of DA-PY/CB[8] under air (green) and after vacuum deoxy (red).

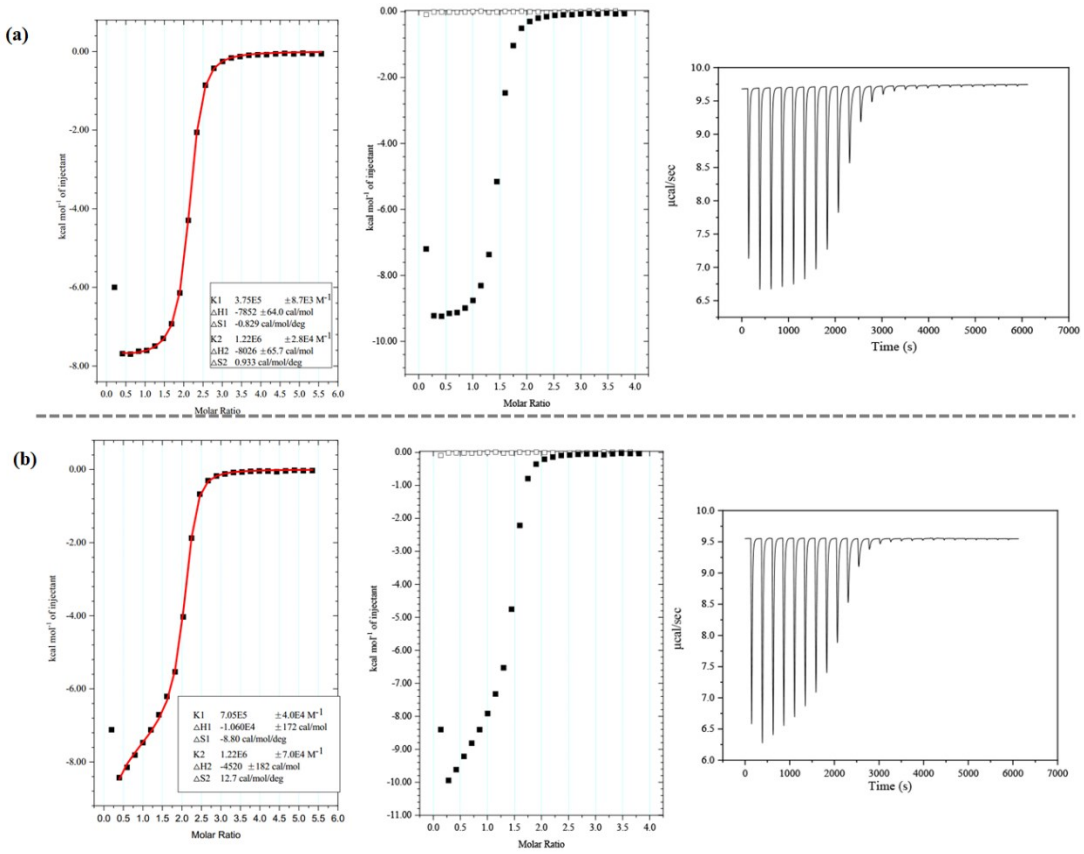

Figure S24. Top: ITC data for MA-PY with CB[8] in H_2O, [CB[8]] (cell) = 0.05 mM, [MA-PY] (syringe) = 1 mM, 298 K; Bottom: ITC data for DA-PY with CB[8] in H_2O, [CB[8]] (cell) = 0.05 mM, [DA-PY] (syringe) = 1 mM, 298 K.

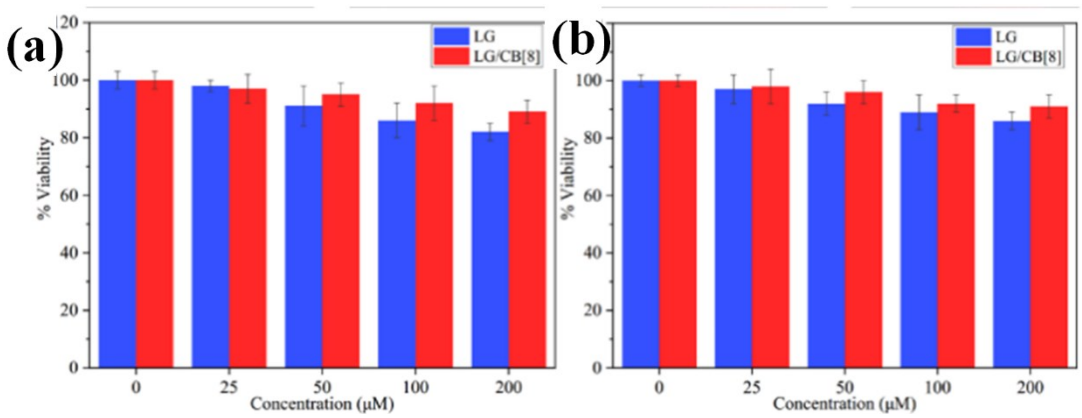

Figure S25. The concentration dependent MTT assay of DA-PY/CB[8] and DA-PY (with different concentration): (a) cancer cells (A549); (b) normal cells (NIH3T3).

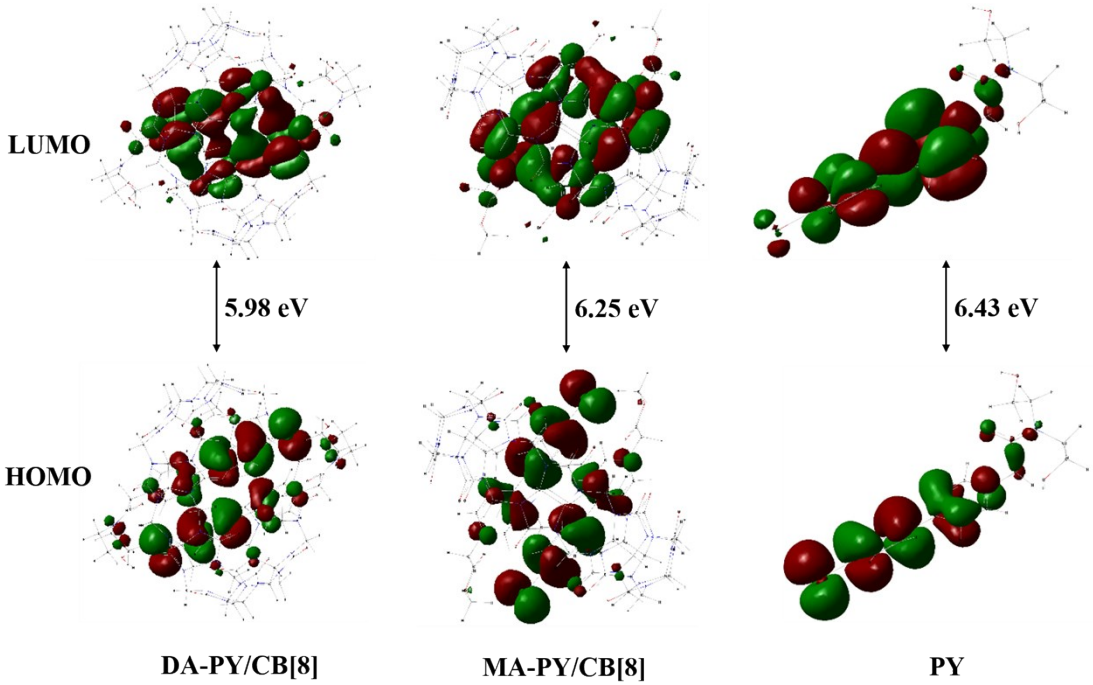

Figure S26. Frontier molecular orbital (FMO) of DA-PY/CB[8], MA-PY/CB[8] and DA-PY.

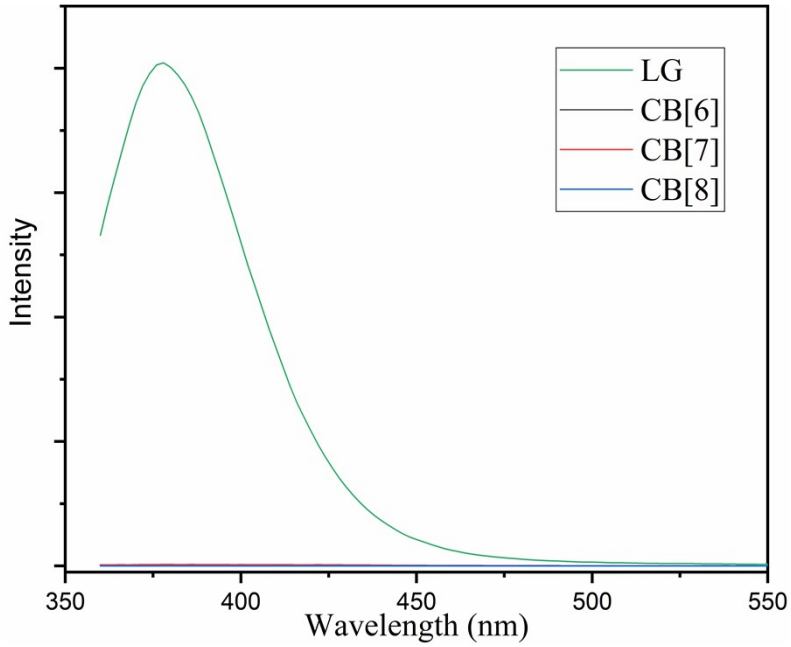

Figure S27. Fluorescence emission spectra in aqueous solution of DA-PY, CB[6], CB[7] and CB[8] at 298K ([DA-PY] = [CB[6]] = [CB[7]] = [CB[8]] = 0.10 mM).

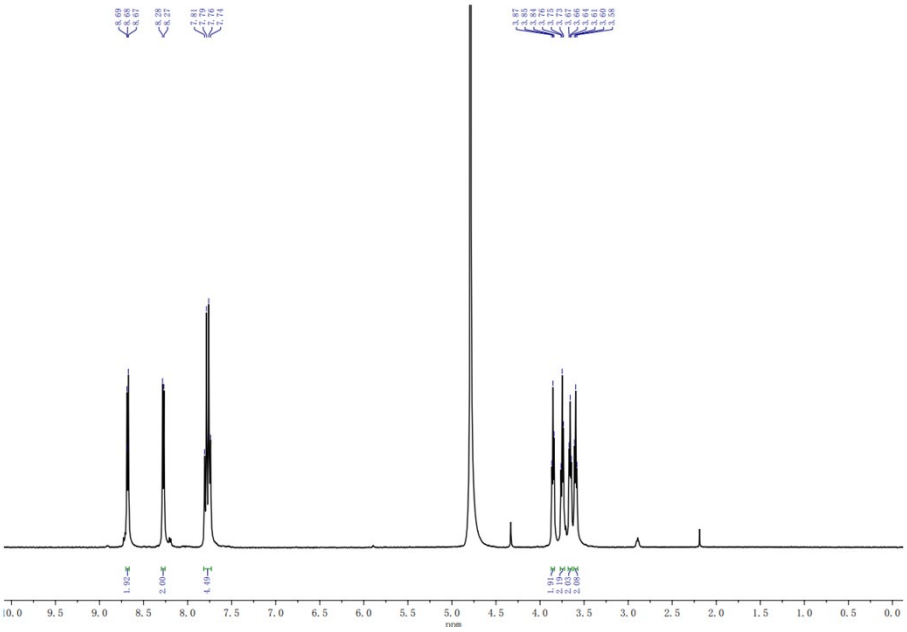

Figure S28. ^{1}H NMR (400 MHz, D_2O, 298 K) spectrum of DA-PY.

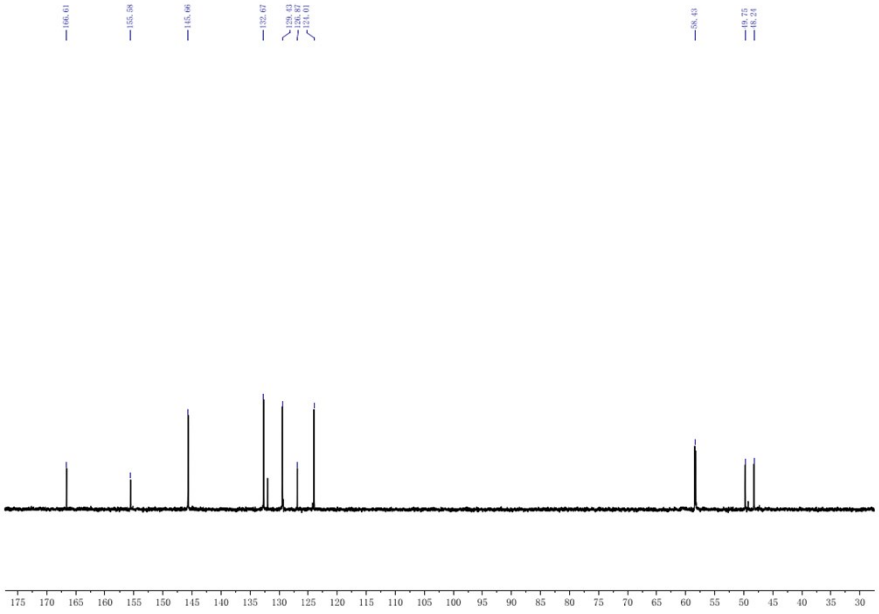

Figure S29. ^{13}C NMR (101 MHz, D_2O, 298 K) spectrum of DA-PY.

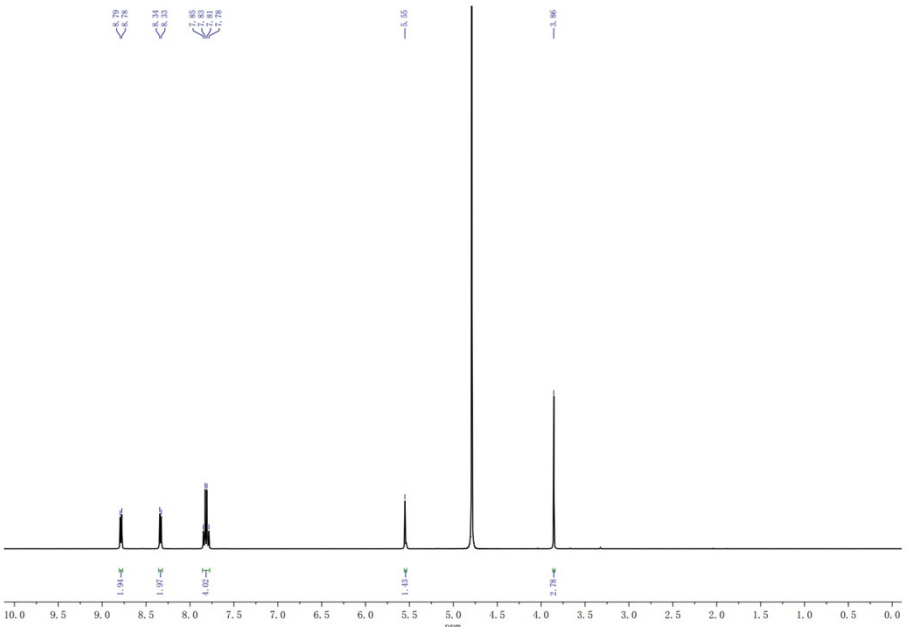

Figure S30. ^{1}H NMR (400 MHz, D_2O, 298 K) spectrum of MA-PY.

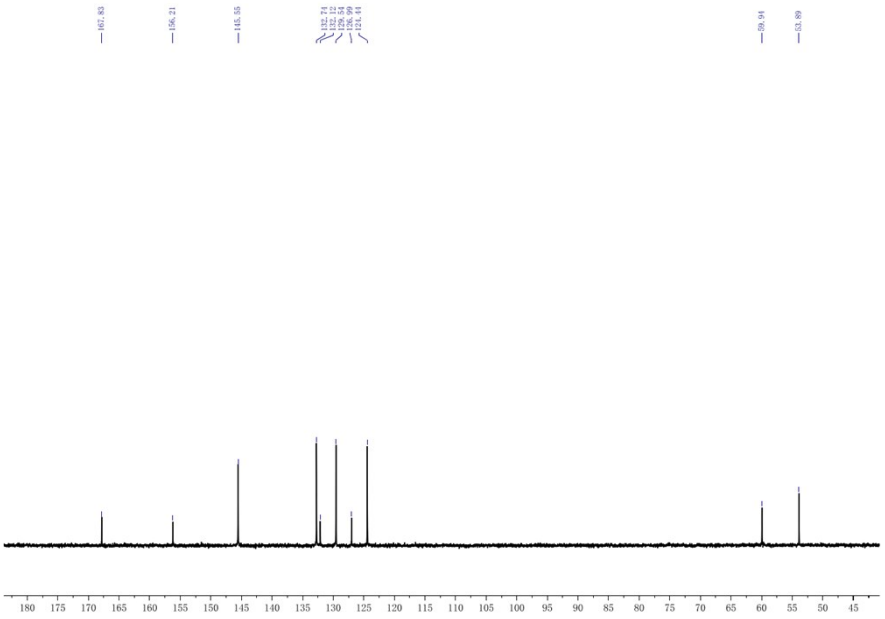

Figure S31. ^{13}C NMR (101 MHz, D_2O, 298 K) spectrum of MA-PY.

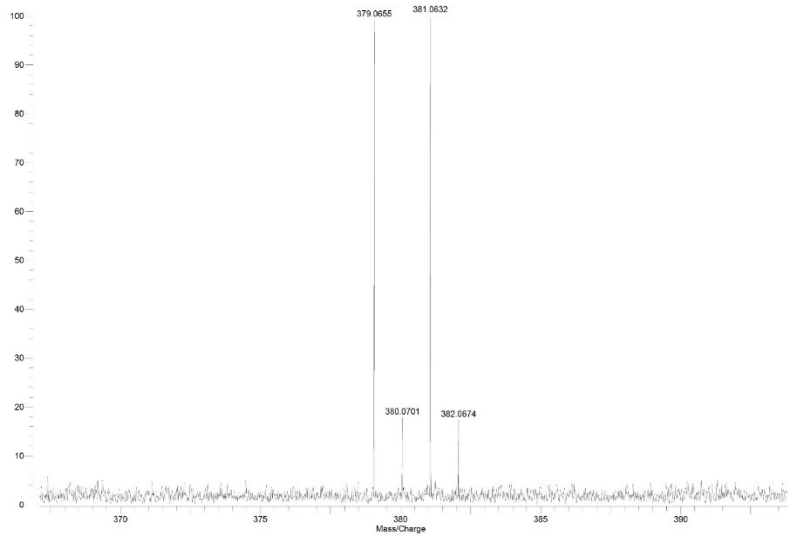

Figure S32. HRMS (ESI) spectrum of DA-PY.

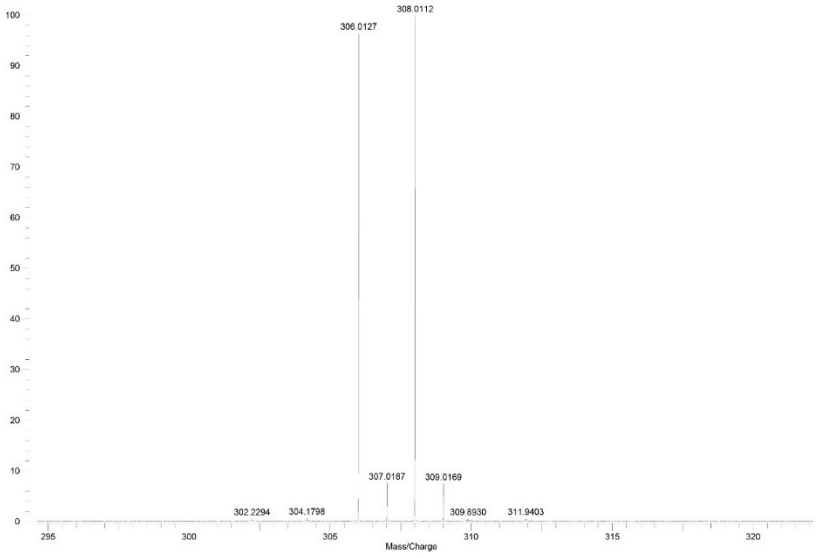

Figure S33. HRMS (ESI) spectrum of MA-PY.

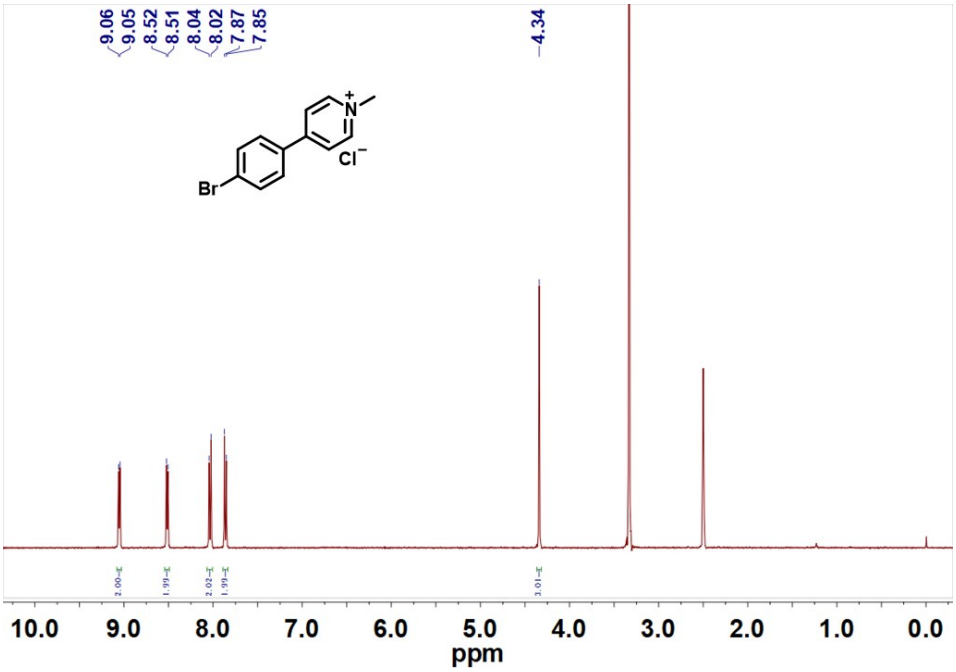

Figure S34. ^{1}H NMR (400 MHz, D_2O, 298 K) spectrum of PY.

REFERENCES

1. Y. Zhao and D. G. Truhlar, Theor. Chem. Acc., 2008, 120, 215–241; (b) Y. Zhao and D. G. Truhlar, *Acc. Chem. Res.* **2008**, *41*, 157-167.
2. S. Grimme, J. Antony, S. Ehrlich and H. Krieg, "A consistent and accurate ab initio parameterization of density functional dispersion correction (DFT-D) for the 94 elements H-Pu," *J. Chem. Phys.* 2010, **132**, 154104.
3. P. C. Hariharan and J. A. Pople , *Theor. Chim. Acta*, 1973, **28**, 213-222.
4. A. V. Marenich , C. J. Cramer and D. G. Truhlar , *J. Phys. Chem. B.* 2009, **113** , 6378.
5. M. J. Frisch, G. W. Trucks, H. B. Schlegel, G. E. Scuseria, M. A. Robb, J. R. Cheeseman, G. Scalmani, V. Barone, G. A. Petersson, H. Nakatsuji, X. Li, M. Caricato, A. V. Marenich, J. Bloino, B. G. Janesko, R. Gomperts, B. Mennucci, H. P. Hratchian, J. V. Ortiz, A. F. Izmaylov, J. L. Sonnenberg, D. Williams-Young, F. Ding, F. Lipparini, F. Egidi, J. Goings, B. Peng, A. Petrone, T. Henderson, D. Ranasinghe, V. G. Zakrzewski, J. Gao, N. Rega, G. Zheng, W. Liang, M. Hada, M. Ehara, K. Toyota, R. Fukuda, J. Hasegawa, M. Ishida, T. Nakajima, Y. Honda, O. Kitao, H. Nakai, T. Vreven, K. Throssell, J. A. Montgomery, Jr., J. E. Peralta, F. Ogliaro, M. J. Bearpark, J. J. Heyd, E. N. Brothers, K. N. Kudin, V. N. Staroverov, T. A. Keith, R. Kobayashi, J. Normand, K. Raghavachari, A. P. Rendell, J. C. Burant, S. S. Iyengar, J. Tomasi, M. Cossi, J. M. Millam, M. Klene, C. Adamo, R. Cammi, J. W. Ochterski, R. L. Martin, K. Morokuma, O. Farkas, J. B. Foresman, and D. J. Fox, Gaussian 16, Revision A.03, Gaussian, Inc., Wallingford, CT, 2016.
6. Neese, F. The ORCA Program System. *Wiley Interdiscip. Rev. Comput. Mol. Sci*. 2012, **2**, 73-78.